# Microbial and catalytic degradation of synthetic dyes

N. Shukova<sup>1\*</sup>, N. Armenova<sup>1</sup>, D. Uzun<sup>2</sup>, A. Gigova<sup>2</sup>, O. Dimitrov<sup>2</sup>, M. Dimtrova<sup>2</sup>, L. Ljutzkanov<sup>1</sup>, E. Razkazova-Velkova<sup>1</sup>

<sup>1</sup>Institute of Chemical Engineering, Bulgarian Academy of Sciences, Acad. G. Bonchev Str., Bl.103, Sofia 1113, Bulgaria

2Institute of Electrochemistry and Energy Systems "Acad. Evgeni Budevski", Bulgarian Academy of Sciences, Acad. G. Bonchev Str., Bl.10, Sofia 1113, Bulgaria

Received: May 01, 2025; Accepted: June 05, 2025

The present work is dedicated to microbial and catalytic degradation of synthetic dyes. Methylene blue, congo red, methyl orange are used as model solution of dyes. A test for cytotoxicity is conducted using two bacterial strains *Pseudomonas putida 1046* and *Bradyrhizobium japonicum 273*. These bacterial strains show tolerance to the dyes up to concentrations of 250 mg/l. It is proved that *Bradyrhizobium japonicum 273* does not decolor the dyes, except for congo red. *Pseudomonas putida 1046* decolors methylene blue and congo red with concentration of 250 mg/l for 42 h up to 96% and 92%, respectively. A screening for an appropriate catalyst for dyes degradation is conducted among ZnO, TiO<sub>2</sub>, ZrO<sub>2</sub> incorporated on a matrix of activated carbon and sole activated carbon. TiO<sub>2</sub> proved to be suitable for the process. Experiments with TiO<sub>2</sub> under different conditions are carried on. *Pseudomonas putida 1046* shows tolerance in the presence of TiO<sub>2</sub>, so experiments for simultaneous microbial and catalytic degradation of methylene blue are conducted.

**Keywords:** Degradation of dyes, *Pseudomonas putida 1046, Bradyrhizobium japonicum 273,* ZnO-, TiO<sub>2</sub>-, ZrO<sub>2</sub>-catalysts.

#### INTRODUCTION

In recent decades, the pollution of water bodies by huge volumes of untreated industrial wastewater (e.g. paper, cosmetics, textiles, plastics, etc.) contaminated with organic dyes, is considered an ecological crisis with a dangerous impact. Wastewaters polluted with dyes are a major restriction for the sustainable development of many industries [1].

Azo dyes make up approximately 60 % of the total dye production per year [2]. They are a class of synthetic chemical compounds characterized by their azo group (-N = N-) and complex aromatic structures [3]. These groups impart vivid colors to the dyes that create strong desires for a number of industrial applications. Azo dyes present high chemical stability and persistence, increasing the challenges to their degradation. The azo dyes are characterized and compared based on their molecular structure and weight, water solubility, acid dissociation constant, n-octanol-water partition coefficient, and maximum absorbance. Congo red (CR) is a diazo dye [4]. Methylene blue (MB) is one of the most common cationic phenothiazine dyes. Methyl orange (MO) is an anionic azo dye, most commonly used for dyeing cotton, wood, and silk. Organic dyes MB and MO have poor biodegradability, meaning that they can remain in

natural water bodies for a long time [5-8].

The methods used for dye removal include chemical, physical and biological processes [9, 10]. Chemical treatments involve oxidation, reduction, and neutralization processes, while physical methods include adsorption, coagulation, and membrane filtration. Biological treatment, involving a combination of microorganisms that break down pollutants, offers a more sustainable and environmentally friendly alternative. Various physicochemical methods are used for treatment of textile wastewaters, but they generate large amounts of toxic sludges which require additional treatment and costs. Heterogeneous photocatalysis offers significant advantages over other methods, mainly low energy consumption, easy operation, no secondary pollution, and moderate reaction conditions. Therefore, the textile industry needs a wastewater treatment technology that removes toxic sludge, requires less energy and remains safe for the environment.

Various adsorbent materials have been tested for the effective removal of methylene blue (MB) including spent olive stones [11] and raw dolomite [12]. Activated lignin-chitosan extruded (ALiCE) pellets offer great potential for removing cationic organic pollutants from rivers and streams [13].

Heterogeneous photocatalysis, using metal oxide semiconductors as photocatalysts, offers a promising

<sup>\*</sup> To whom all correspondence should be sent: E-mail: *nastemi1@abv.bg* 

alternative for degrading toxic organic pollutants into harmless inorganic molecules. Metal oxide semiconductors such as TiO<sub>2</sub> [14], ZnO [15, 16], NiO [17, 18], CuO [19], MnO<sub>x</sub> [20, 21] and Cr<sub>2</sub>O<sub>3</sub> [22] are used as catalysts. They are promising materials due to their electronic structure, light absorption properties, and charge transport characteristics [23]. They have outstanding physical, chemical, and optical properties. They are costeffective and non-toxic catalysts that allow complete mineralization. The (Mn, Ni) co-doped ZnO catalyst is prepared using Stephania abyssinica leaf extract [16] and is used for degradation of MB dye under visible light. TiO<sub>2</sub>-g-C<sub>3</sub>N<sub>4</sub> heterojunction is employed as a photocatalyst for the sunlight-assisted photodegradation of CR dye [18]. Nickel-doped zinc oxide (Ni<sub>0.05</sub>Zn<sub>0.95</sub>O) nanoparticles are tested as a potential adsorbent and catalyst for the removal of specific dves, MO and tartrazine, from an aqueous solution [24]. Co<sub>3</sub>O<sub>4</sub> nanocube-doped polyaniline nanocomposites have been successfully synthesized as an oxidant in acidic medium for efficient removal of MO from aqueous solution [25].

Different strains are reported to degrade azo dyes [26]. In [27] *Pseudomonas mt2* degrades MO dye. *Bradyrhizobium japonicum* and *Pseudomonas putida* are reported [28, 29] to degrade phenol and cathehin that are intermediate products of dye mineralization.

Many papers are dedicated to the decolorization of azo dyes in fuel cells [30, 31]. The microbial fuel cells (MFCs) combine physiochemical and

biological principles to convert chemical waste into electric energy and detoxify pollutants. Waste pomelo peel is used as the main raw material for preparation of iron-nitrogen-carbon nanocomposite as cathode catalyst for the degradation of CR in a fuel cell [30].

The aim of the present work is to study the catalytic and microbial degradation of MO, MB and CR. MO and CR are chosen as models of anionic azo dyes and MB as a cationic one. These are preliminary investigations in order to choose an appropriate catalyst and strain for further development of a fuel cell for dyes decontamination.

### MATERIALS AND METHODS

The biomass concentrations read as optical densities (OD) and dye concentrations are determined spectrophotometrically on a VWR UV–1600 PC spectrophotometer at a wavelength of 600 nm for the biomass, 664 nm for MB, 498 nm for CR and 465 nm for MO. The rate of the decolorization is calculated by the following equation:

% decolorization = 
$$\frac{A_0 - A_{\text{sample}}}{A_0} \times 100$$
, where

 $A_o$  – absorption of the beginning solution;  $A_{sample}$  – absorption of the tested sample.

The experiments are conducted with dyes (Merck KGaA) dissolved in a phosphate buffer solution. Summarized information of the dyes is given in Table 1.

**Table 1.** Information about the investigated dyes

Name of the azo dye	Chemical formula	Molecule structure	Characteristic
Methylene blue (MB)	C <sub>16</sub> H <sub>18</sub> ClN <sub>3</sub> S	S N N CI	Cationic azo dye
Methyl orange (MO)	C <sub>14</sub> H <sub>14</sub> N <sub>3</sub> NaO <sub>3</sub> S	N = N = N	Monoazo anionic acid dye
Congo red (CR)	$C_{32}H_{22}N_6Na_2O_6S_2$	NH <sub>2</sub> NH <sub>2</sub> N=N N=N N=N N=N N=N	Diazo anionic direct dye

### Catalysts preparation

All catalysts are incorporated on a matrix of activated carbon. Their preparation method is a patented technology that includes impregnation of organic material with the corresponding precursor salt and subsequent pyrolysis with simultaneous activation [32]. ZnO, TiO2, ZrO2 incorporated on a matrix of activated carbon and sole activated carbon are used in this investigation. The organic material for the preparation of the catalysts are sunflower husks. The catalyst showing the best performance (namely TiO<sub>2</sub>) is characterized by SEM, EDS, XRD, surface area by BET and iodine adsorption. BET studies are carried out employing a Quantachrome instrument Autosorb iQ (USA) that measures the quantity of gas adsorbed on or desorbed from a solid surface at an equilibrium vapor pressure by a static volumetric method. The investigations are carried out on NOVAtouch-Quantachrome instrument apparatus (USA) that measures adsorbed and desorbed volumes of gas at relatively low pressure (lower than 1). The obtained data after computer processing are presented as isotherms of adsorption and/or desorption from which are calculated specific surface area, pore volume, pore size and pore size distribution of the powder samples. X-ray diffraction (XRD) patterns are recorded utilizing a diffractometer using CuKa radiation  $(\lambda=1.54178 \text{ Å}, 40 \text{ kV} \text{ and } 30 \text{ mA})$  with a scanning rate of 2° min<sup>-1</sup>. The surface morphology of the samples is investigated by scanning electron microscopy (SEM) using a Zeiss Evo 10 microscope (Carl Zeiss Microscopy, Oberkochen, Germany). The images are taken in secondary electrons mode with accelerating voltage of 25 keV, and no additional conductive coating on the surface. The chemical composition of the samples is studied using the Oxford Ultim Max 40 electron dispersive spectroscopy (EDS) probe (Oxford Instruments, Abingdon, UK). The results are compiled with AZtec software (version 6.1 HF4).

## Catalytic decolorization

The conditions for the catalytical decolorization are 200 ml dye solution and 0.1 g catalyst. Screening for the most appropriate catalyst is conducted. Different conditions are investigated as rpm, dark and light mode, etc.

Microbial strain and cultivation conditions

The bacterial strains *Pseudomonas putida* (NBIMCC 1046) and *Bradyrhizobium japonicum* 273, used for the decolorization assays, are obtained

from the Bulgarian National Bank for Industrial Microorganisms and Cell Cultures. The bacterial strains are maintained as a frozen liquid culture supplemented with 1:1 glycerol at -20 °C

The strain *P. putida* is cultured in 500 ml flasks with 100 ml of medium containing: peptone – 10 g/l, meat extract – 10 g/l, NaCl – 5 g/l. The inoculum for the experiments is developed up to  $OD_{600} = 2$  at 30 °C per shaker and 100 rpm.

*B. japonicum* is cultured in 500 ml flasks with 100 ml. of YMA (yeast mannitol agar) medium containing - K<sub>2</sub>HPO<sub>4</sub> - 0.2 g/l, MgSO<sub>4</sub> - 0.2 g/l, mannitol - 10 g/l, yeast extract - 0.3 g/l, NaCl -20 g/l for 7 days at 28 °C.

For the investigation for tolerance of the strains to different dye concentrations, the cultivation is conducted by adding 20 g/l agar to the abovementioned cultivation media.

Azo dyes with different concentrations (100 mg/l - 250 mg/l) are dissolved in phosphate buffer and sterilized trough 0.45 µm filter. The tolerance of the bacteria to azo dye is studied by the "hole method" in a Petri dish [33]. A sterilized cork borer is used to create the wells (8 mm in diameter). The azo dye solutions (80 µl) with different concentrations (100 mg/l - 250 mg/l) are introduced in the lateral 4 holes. Holes in the center of the agar plate filled with sterile phosphate buffer solution (80 µl) are used as control. Petri dishes are incubated in a thermostat for 24 h (P. putida) at +30 °C / or 7 days (B. japonicum) at +28°C. The inhibition diameter is measured and the minimum inhibitory concentration is determined. The experiments for dye decolorization are carried out with 10% (v/v) inoculation of the bacterial stains in 500 ml flasks with 200 ml of dye solution and the components of the respective cultivation media on a rotary shaker at 30 °C and a stirring speed of 100 rpm. Periodically samples for decolorization of the dyes are centrifuged (10 000 rpm, 5 min) and the absorbance of the supernatants is measured at 664 nm for MB, 498 nm for CR, 465 nm for MO.

Experiments for the tolerance of P. putida to the  $TiO_2$  catalyst are performed using two parallel cultivations with and without catalyst. No inhibition of the growth in the presence of  $TiO_2$  is observed. The quantity of the catalyst is the same as for the experiments for the catalytic decolorization.

### RESULTS AND DISCUSION

The results for decolorization using different dyes and catalysts are summarized in Table 2. The experiments are carried out with dye concentration of 120 mg/l for 5 days without stirring at a temperature of 25 °C. It can be seen that TiO<sub>2</sub> and

ZnO have the best performance. In Table 3 a comparison of TiO<sub>2</sub> and ZnO for decolorization of MB at 25 °C for 4 days is given. The results are for dyes dissolved in buffer and in distilled water under stirring with different speeds and without stirring. The results show a slight dependence of the decolorization rate on the rotation speed and the solvent used.

Table 2. Comparison of different catalyst

Dye Catalyst, surface area, m²/g*	MO, % of decolorization	MB, % of decolorization
ZnO, 645	96.5	98.82
TiO <sub>2</sub> , 798.	98	99.95
ZrO <sub>2</sub> , 503	50	43
Activated carbon (AC), 310	43	39

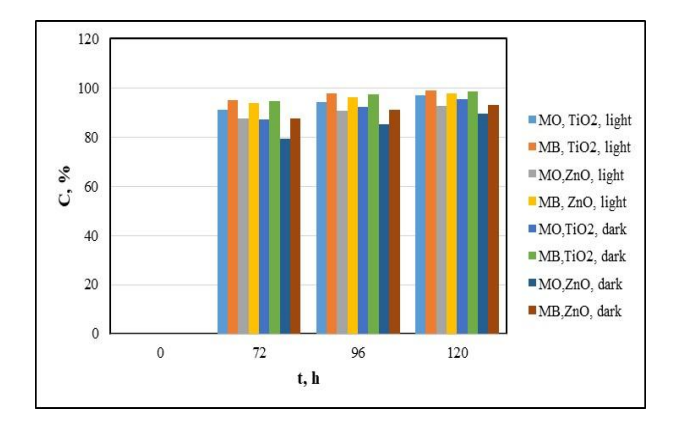
<sup>\*</sup>Surface area by iodine adsorption

Table 3. Comparison of  $TiO_2$  and ZnO catalysts at different conditions

	Decolorization of dye dissolved in water, %			Decolorization of dye dissolved in phosphate buffer, %		
	Without stirring	100 rpm	150 rpm	Without stirring	100 rpm	150 rpm
TiO <sub>2</sub>	94.40	98.2	99.96	97.85	95.1	99.6
ZnO	91.35	92.2	98,4	99.4	93.1	99.5

Fig. 1 represents the decolorization rate using TiO<sub>2</sub> and ZnO in light and dark mode. The initial concentration of the dyes is 100 mg/l. The solution is prepared in phosphate buffer. As it can be expected, the decolorization is slower at dark mode.

Once again, the performance characteristic of TiO<sub>2</sub> exceed those of ZnO.



**Fig. 1**. Comparison of the decolorization of dyes with different catalysts and conditions

 $TiO_2$  was chosen for further investigations. The SEM images of  $TiO_2$  on sunflower husks are shown in Fig. 2.

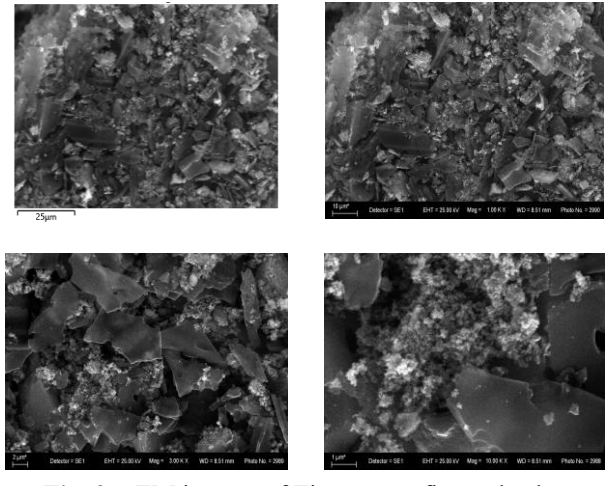


Fig. 2. SEM images of TiO<sub>2</sub> on sunflower husks

The EDS results are shown in Fig. 3 and summarized in Table 4.

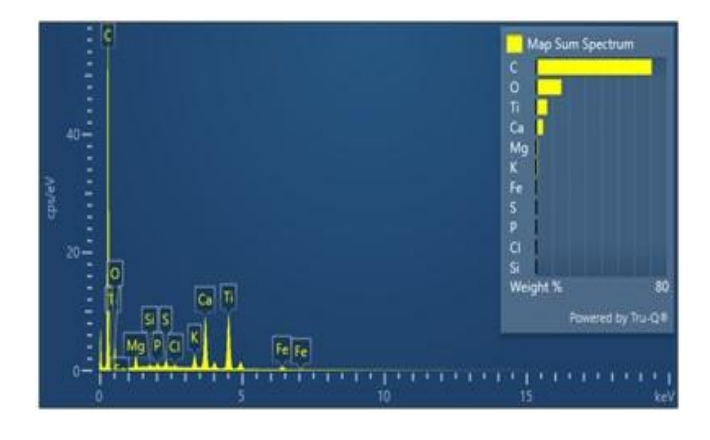




Fig. 3. EDS of the  $TiO_2$  on sunflower husks.

Table 4	Results	of the ED	S of the	TiO <sub>2</sub> o	n sunflower husks
I able 4	. IXCSUIIS	or the LL	o or me	11070	n summo wei musks

Map Sum Spectrum					
Element	Signal Type	Line	Wt%	Wt% Sigma	Atomic %
С	EDS	K series	70.77	0.13	81.97
О	EDS	K series	15.36	0.13	13.36
Mg	EDS	K series	0.96	0.01	0.55
Si	EDS	K series	0.09	0.01	0.04
P	EDS	K series	0.18	0.01	0.08
S	EDS	K series	0.35	0.01	0.15
Cl	EDS	K series	0.11	0.01	0.04
K	EDS	K series	0.89	0.01	0.31
Ca	EDS	K series	4.06	0.02	1.41
Ti	EDS	K series	6.57	0.03	1.91
Fe	EDS	K series	0.66	0.01	0.16
Total			100.00		100.00

The surface morphology of the catalytic powder and its chemical composition are characterized by SEM and EDS techniques (Figs. 2, 3). The SEM images reveal that the morphology of the powder consists of two distinctive components - larger flat substrates with smaller clustered particles on top and between them. The large plate-like structures with irregular shapes and sizes between 5-20 µm form the base the catalytic powder. of The measurements clearly show that they are made of carbon and a closer look at higher magnifications reveals that they serve as a substrate for the nanocomponent of the catalyst. According to the elemental analysis, the small uniform particles (20-30 nm) that can be found clustered in the gaps of the carbon plate structures are primarily made of titanium and oxygen. This is in agreement with the XRD analysis that showed the presence of a tetragonal TiO2 phase. The observed surface morphology of nano sized particles on substrates with large surface area facilitates good catalytic properties of the synthesized material. The other element that can be seen from the elemental maps occupying the same volume as titanium in the powder is calcium. According to the XRD it forms the second distinctive phase in the catalyst, rhombohedral full chemical CaCO<sub>3</sub>. The composition of the powder is calculated from the EDS results and can be viewed in Table 4. As expected, the strongest signal is attributed to carbon which comes from the sunflower husks. Oxygen accounts for about 13 at. %, followed by Ti and Ca with 1.9 and 1.4 at. %, respectively. All other elements are registered in very small amounts in the powder (under 0.5 at. % each) and can be attributed

to precursor impurities and sunflower husk inclusions.

A PANalytical Aeris diffractometer with CuK $\alpha$  radiation (40 kV, 15 mA), wavelength  $\lambda$ =1.5406 Å and  $\theta$ - $\theta$  Bragg-Brentano geometry is used to determine the phase composition. The diffractogram is taken at room temperature, constant scan rate and reflection angle 2 $\theta$  in the range 10÷70° with a step of 0.02°, 60 s. The resulting XRD pattern is interpreted using the PDF 2-2022 database, ICDD. The presented diffractogram reveals the phase composition of the TiO<sub>2</sub> catalyst (Fig. 4).

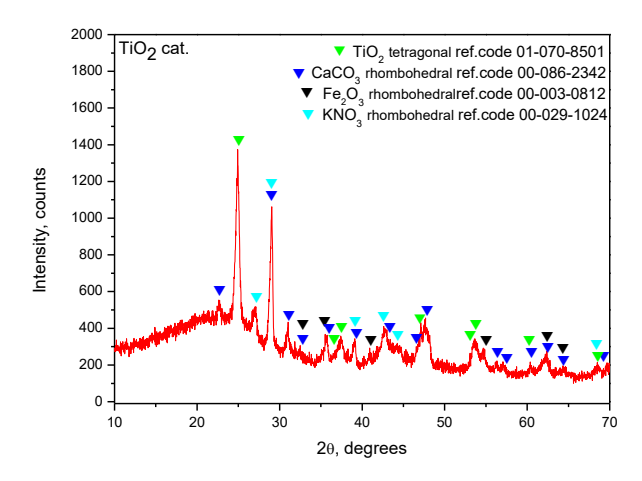
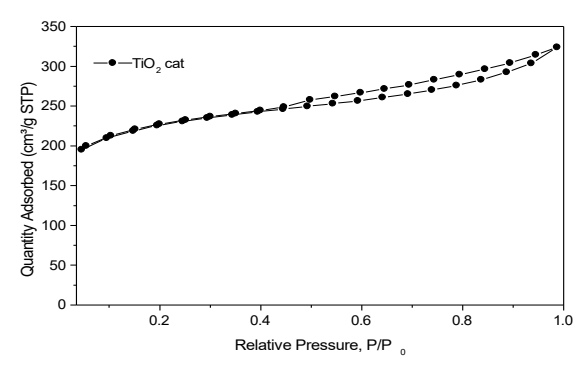


Fig. 4. XRD of TiO<sub>2</sub> on sunflower husks

The synthesized material exhibits low crystallinity, with the presence of an amorphous halo likely attributed to the use of an activated carbon carrier (derived from sunflower husks). The most intense peak, recorded at  $2\theta = 24.76^{\circ}$ , along with additional peaks at  $37.38^{\circ}$ ,  $46.89^{\circ}$  and  $53.13^{\circ}$ , is associated with the (101), (004), (200), and (105) crystallographic planes of the tetragonal  $TiO_2$ 

structure. The peak at  $2\theta = 29.02^{\circ}$ , attributed to the primary (104) reflection of the rhombohedral CaCO<sub>3</sub> phase, together with smaller peaks at 22.63°, 30.99°, 36.06° and 39.33°—linked to the (102), (006), (110), and (113) planes, respectively – confirm its significant presence in the catalyst. Additionally, the emergence of lower-intensity peaks at  $2\theta = 54.58^{\circ}$  and 27.02°, corresponding to the (122) and (012) orientations of the rhombohedral Fe<sub>2</sub>O<sub>3</sub> and KNO<sub>3</sub> phases, respectively, suggests that these two phases are present in smaller amounts within the TiO<sub>2</sub> catalyst.

The adsorption and desorption isotherms of TiO<sub>2</sub> catalyst are measured by physisorption of nitrogen gas. The isotherms are presented in Fig. 5.



**Fig. 5.** Nitrogen adsorption/desorption isotherms on TiO<sub>2</sub> catalyst

The measured sorption isotherm approaches Type I (b) according to the IUPAC classification, with H4 type hysteresis. Reversible isotherms of this Type are given by microporous solids. For nitrogen adsorption at 77 K, Type I (b) isotherms are found with materials having pore size distributions over a broader range including wider micropores and possibly narrow mesopores ( $< \sim 2.5$  nm). The H4type hysteresis loop is often found in micromesoporous carbons [34]. The structural characteristics are determined from the adsorption isotherm and are summarized in Table 5.

Table 5. Surface characteristics of TiO2

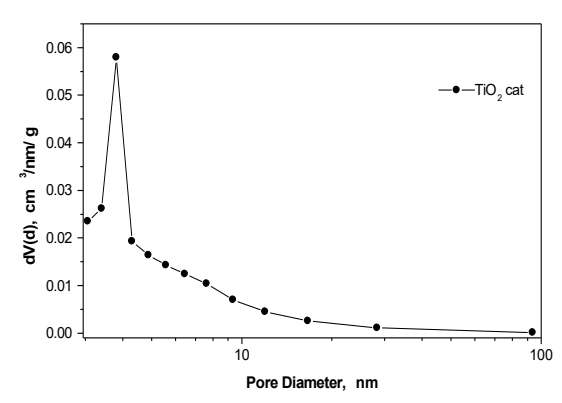
Characteristics	TiO <sub>2</sub> catalyst	
Surface area (BET), m <sup>2</sup> /g	722	
Pore volume, cm <sup>3</sup> /g	0.502 for pores smaller than 150 nm (D)	
Average pore diameter, (4V/S), nm	2.8	
*Pore diameter (BJH desorption), nm	3.8	

<sup>\*</sup>The pore diameter is reported from the desorption isotherm.

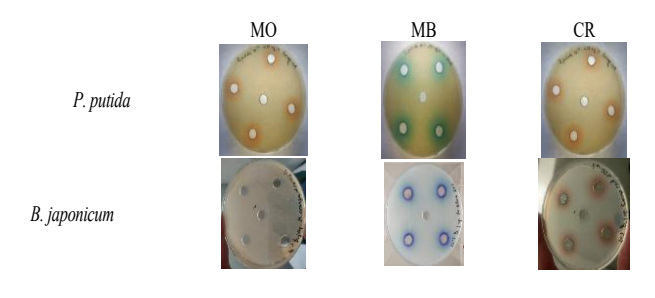
The surface area is determined by the BET (Brunauer, Emmett, Teller) method. Multipoint BET is defined at relative pressure in the range of  $p/p_0 =$ 0.1 - 0.3. The pore volume is measured at a relative pressure close to 1 (p/p<sub>0</sub> = 0.99). Average pore diameter is calculated, assuming that the pores have a cylindrical geometry at  $p/p_0 = 0.99$ . The measured structural characteristics of the TiO2 catalyst studied show a large specific surface area and a developed pore volume for pores with a diameter below 150 nm. The average pore diameter is 2.8 nm, close to the diameter of the most common pores with a size of 3.8 nm (see Fig. 6). Pore size distribution is the distribution of pore volume with respect to pore size. In this case, the pore diameter distribution is calculated from the desorption branch of the isotherm using the Barrett, Joyner, Halenda method (BJH method, Desorption). The differential pore diameter distribution curve for TiO2 catalyst is given in Fig. 6. The peak is at a pore diameter of 3.8 nm.

Fig. 7 shows the tolerance of both strains to the maximal concentration of the dyes. Up to the studied concentrations, no inhibition zone is detected.

Fig. 8 shows the decolorization of MB and CR for 42 h with *P. putida*. The initial concentration is 250 mg/l. The decolorization rate at 42 h is 92 % for CR and 96 % for MB. *B. japonicum* doesn't degrade MB and MO. It degrades CR to 95 % for 72 h.



**Fig. 6.** Differential pore diameter distribution curve of TiO<sub>2</sub> catalyst



**Fig. 7.** Tolerance of the bacterial strains to 250 mg/l of the dyes

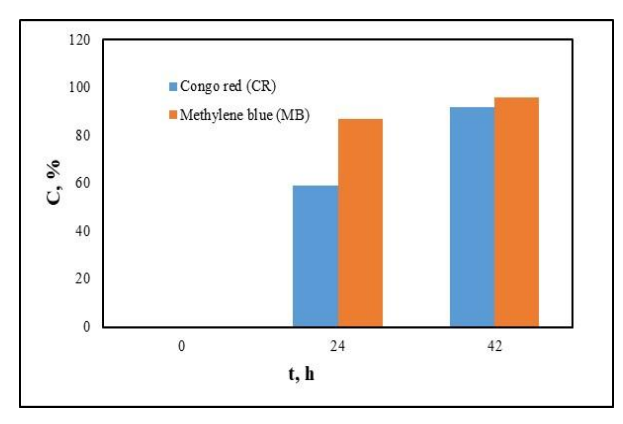
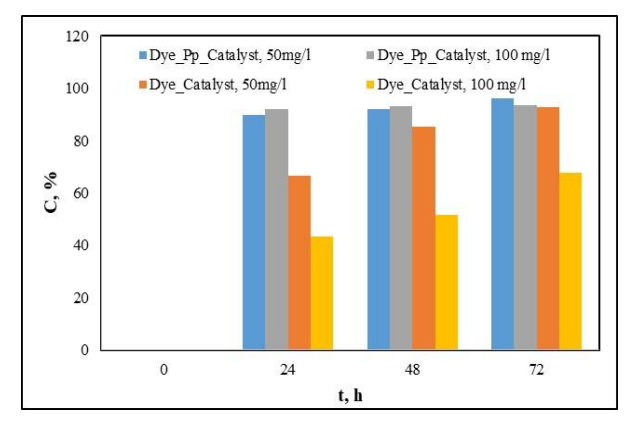


Fig. 8. Decolorization of dyes with *Pseudomonas* putida 1046

Fig. 9 shows a comparison of the decolorization rate of MB by the use of catalyst and combination of P. putida and catalyst at two different dye concentrations (100 mg/l and 50 mg/l). The combination of a catalytic and a bacterial process gives about two times faster decolorization for the 24<sup>th</sup> hour for both concentrations as compared with the pure catalyst. For the 48<sup>th</sup> hour the rate is also two times higher for the higher concentration. The decolorization rate at the 72<sup>nd</sup> hour is 93 % for the lower concentration and 94 % for the higher in the presence of bacteria and only 68 % for the higher concentration with catalyst. Further investigations are going to be carried out with different concentrations of dye in order to estimate the synergetic effect of catalyst and bacteria and the concentration that can be decolorized by the bacteria.



**Fig. 9.** Comparison of the decolorization of MB at different conditions with *P. putida 1046* (Pp).

# CONCLUSIONS

It is found that the dyes are not toxic to *Pseudomonas putida 1046* and *Bradyrhizobium Japonicum 273 up to a* concentration of 250 mg/l. *Bradyrhizobium Japonicum 273* does not degrade the studied dyes, except CR. *Pseudomonas putida* 

1046 can decolorize 250 mg/l of MB and CR for 42 h. up to 92 % and 96 % respectively.

The comparison of ZnO and TiO<sub>2</sub> as catalysts for dye degradation shows the advantage of TiO<sub>2</sub> as a catalyst. TiO<sub>2</sub> is not toxic to *Pseudomonas putida 1046*. The decolorization of MB in the presence of TiO<sub>2</sub> and *Pseudomonas putida* 1046 is 90 % for 24 h while using only the catalyst it is 40-60 % for the same time.

Acknowledgement: This research was funded by the Bulgarian National Science Fund, grant number KP-06-N67/6 from 12 December 2022.

#### REFERENCES

- 1. W.S. Wan Ngah, L.C. Teong, M.A.K.M. Hanafiah, *Carbohydr. Polym.*, **83**, 1446 (2011).
- H. D. Bouras, A. R. Yeddou, N. Bouras, D. Hellel, M. D. Holtz, N. Sabaou, A. Chergui, Nadjemi, J. Taiwan Inst. Chem. Eng., 80, 915 (2017) DOI: 10.1016/j.jtice.2017.08.002.
- M. Sharma, S. Sharma, A. Ahmed, M. Alkhanjaf, N. K. Arora, B. Saxena, A. Umar, A. A. Ibrahim, M. S. Akhtar, A. Mahajan, S. Negi, R. Kumar, S. Baskoutas, J. of Ind. and Eng. Chem. 142 45, (2025).
- 4. A. Strebell, M. Behringer, H. Hilbig, A. Machner, B. Helmreich, *Frontiers in Environ. Eng.*, DOI 10.3389/fenve.2024.1347981 1, (2024).
- A. Asfaram, M. Ghaedi, S. Hajati, A. Goudarzi, RSC Adv. 5, 72300 (2015).
- 6. Y. Liu, Z. Chen, C.-H. Shek, C.M.L. Wu, J.K.L. Lai, *ACS Appl. Mater. Interfaces*, **6**, 9776 (2014).
- 7. H. Zou, Y. Wang, *Environ. Sci. Pollut. Res.*, **26**, 23061 (2019).
- 8. Y. Yang, W. Yu, S. He, S. Yu, Y. Chen, L. Lu, Z. Shu, H. Cui, Y. Zhang, H. Jin, *App. Clay Sci.*, **168**, 304 (2019).
- 9. Y. Yang, D. Jin, G. Wang, D. Liu, X. Jia, Y. Zhao, *Colloid Surf.*, *B*, **88**, **521** (2011).
- 10. S. Natarajan, H.C. Bajaj, R.J. Tayade, *J. Environ. Sci.*, **65**, 201 (2018), https://doi.org/10.1016/j.jes.2017.03.011.
- A.B. Albadarin, C. Mangwandi, J. Environ. Manage., 164, 86 (2015).
- 12. A.B. Albadarin, J. Mo, Y. Glocheux, S. Allen, G. Walker, C. Mangwandi, *Chem. Eng. J.*, **255**, 525 (2014).
- 13. A. B. Albadarina, M. N. Collinsc, M. Naushad, S. Shirazian, G. Walker, C. Mangwandi, *Chem. Eng. J.*, **307**, 264 (2017).
- F. Di Fonzo, C.S. Casari, V. Russo, M.F. Brunella, A.L. Bassi, C.E. Bottani, *Nanotechnology*, 20, (2008).
- A. Di Mauro, M.E. Fragala, V. Privitera, G. Impellizzeri, *Mater. Sci. Semicond. Process*, 69, 44 (2017).
- 16. H. H. Haitosa, B. B. Tesfamariam, N. S. Gultom, Dong-Hau Kuo, X. Chen, Yi-nan Wu, O. A. Zelekew, *J. of Mol. Liquids*, **368**, 120666 (2022).

- 17. A. Diallo, K. Kaviyarasu, S. Ndiaye, B. Mothudi, A. Ishaq, V. Rajendran, M. Maaza, *Green Chem. Lett. Rev.*, 11, 166 (2018).
- 18. M. Saeed, H. Asghar, I. Khan, N. Akram, M. Usman, *Catalysis Today*, **447**, 115 (2025).
- P. Raizada, A. Sudhaik, S. Patial, V. Hasija, A.A.P. Khan, P. Singh, S. Gautam, M. Kaur, V.-H. Nguyen, Arab. J. Chem., 13, 8424 (2020).
- 20. R. Yang, Y. Fan, R. Ye, Y. Tang, X. Cao, Z. Yin, Z. Zeng, *Adv. Mater.*, **33** (9), e2004862 (2021).
- J. Y. Zheng, J. He, C. B. Han, G. Huang, B. C. Sun, W. K. Zhao, Y. Wang, L. Sun, J. Si, H. Yan, *Int. J. Biol. Macromol.*, 237, 124 (2023).
- 22. J. Su, H. Xue, M. Gu, H. Xia, F. Pan, *Ceram. Int.*, **40**, 15051 (2014).
- 23. M.M. Khan, S.F. Adil, A. Al-Mayouf, *Elsevier*, 462 (2015).
- 24. C. Klett, A. Barry, I. Balti, P. Lelli, F. Schoenstein, N. Jouini, *J. of Environ. Chem. Eng.*, **2** (2), 914 (2014).
- 25. S. Shahabuddin, N. M. Sarih, S. Mohamad, S. N. A. Baharin, *RSC Adv.*, **49**, 1 (2016).

- G. McMullan, C. Meehan, A. Conneely, N. Kirby, T. Robinson, P. Nigam, I. M. Banat, R. Marchant, W. F. Smyth, *Appl. Microbiol Biotechnol.*, 56, 81 (2001) DOI 10.1007/s002530000587.
- 27. T. P. Thao, Hsiang-Chien Kao, Ruey-Shin Juang, J. Chi-Wei Lan, *J. of the Taiwan Inst. of Chem. Eng.*, 44, 780 (2013).
- 28. E. Vasileva, Ts. Parvanova-Mancheva, V. Beschkov, *J. of Int. Scientific Publications*, **14**, 165 (2020).
- 29. W. Hopper, A. Mahadevan, *Biodegradation*, 159 (1997) DOI: 10.1023/A: 1008254812074.
- 30. S. Zhang, Sh. Zhang, H. Liu, L. Li, R. Guo, *J. of Environ. Chem. Eng.*, **11**, 109264 (2023)
- 31. A. Yadav, P. Kumar, D. Rawat, Sh. Garg, P. Mukherjee, F. Farooqi, A. Roy, *Sci. of the Total Environ.*, **826**, 154038 (2022).
- 32. L. Ljutzkanov, A. Atanasov, BG patent № 63594 /26.06.2002.
- 33. N. Vorobey, K. Kukol, P. Pukhtaievych, S. Kots, *J. Central Europe. Agricul.*, **22 (4)**, 735 (2021), https://doi.org/10.5513/JCEA01/22.4.3157.
- 34. M. Thommes, K. Kaneko, A. V. Neimark, J. P. ver, F. R. Reinoso, J. Rouquerol, S. W. S. Kenneth, *Pure and Appl. Chem.*, 1051 (2015) https://doi.org/10.1515/pac-2014-1117.